JOURNAL OF CATALYSIS **175,** 185–193 (1998)
ARTICLE NO. CA982006

Tracer Studies of Olefin Oxidation over an α-$Bi_2Mo_3O_{12}$ Catalyst Using Laser Raman and Microwave Spectroscopy

Takehiko Ono,*[,1] Nobuaki Ogata,*[,2] and Robert L. Kuczkowski†

*Department of Applied Chemistry, Osaka Prefecture University, Sakai, Osaka 599-8531, Japan; and †Department of Chemistry, University of Michigan, Ann Arbor, Michigan 48109-1055

Received July 8, 1997; revised November 26, 1997; accepted January 20, 1998

The oxide oxygen of α-$Bi_2Mo_3O_{12}$ was exchanged via olefin oxidation using $^{18}O_2$. Band shifts in the Raman spectra of the catalyst were examined. In the oxidation of propene and trans-but-2-ene, the bands at 865 and 845 cm^{-1} of α-$Bi_2Mo_3O_{12}$ were shifted preferentially. Oxygen insertion apparently takes place at the vacancies on Mo–O tetrahedra associated with these bands. Four deuterated acrolein species obtained from the oxidation of cis-CHD=CD–CH_3 over α-$Bi_2Mo_3O_{12}$ and MoO_3 catalysts were examined by microwave spectroscopy. The products exhibited an isotope effect for the second hydrogen abstraction. This is consistent with a fast π-allyl to σ-allyl equilibration process over γ-Bi_2MoO_6 as reported previously. These results were discussed with focus on the allyl intermediate associated with the catalyst and the oxide tetrahedra. In particular, specific Mo–O bonds in the α_1 and α_2 tetrahedra are identified as involved in the oxidation process.

1. INTRODUCTION

It is generally accepted that the reaction of oxide ions with alkenes and reoxidation by gaseous oxygen occur in different regions over catalysts such as the Bi–Mo oxides during catalytic oxidations. Several key articles by the Grasselli school summarize their body of work which has contributed much to this understanding (1–6). Snyder and Hill (7) have more recently discussed the involvement of different types of lattice oxygen, for propene oxidation over a γ-Bi_2MoO_6 catalyst from results reported by several groups (8–11). According to these studies, it has been recognized that the initial hydrogen abstraction involves an oxygen atom associated with bismuth producing an allyl intermediate and that the second hydrogen abstraction is facilitated by the presence of molybdenum oxide polyhedra. The proposals about the origin of the oxygen atoms which insert into the allyl intermediate were different in these reports, i.e., the extent of participation from the Mo oxide or Bi oxide in the γ-phase. Grasselli *et al.* (1–5, 36) proposed a rapid π-allyl to σ-allyl equilibration process on molybdenum oxide polyhedra of Bi-molybdate catalysts. Since an α-$Bi_2Mo_3O_{12}$ catalyst does not consist of a layer structure but has two twin Mo tetrahedra and oxygen anions which are connected to both Mo and Bi cations, it seemed worthwhile to probe this system for insights via several isotopic labeling experiments.

Previously, one of the authors (T.O.) has reported that the oxide ions of MoO_3 (12) and scheelite-type molybdate (13) were exchanged with ^{18}O tracer when reduced by butene and reoxidized by $^{18}O_2$. With an α-$Bi_2Mo_3O_{12}$ catalyst (13, 14), the bands in the region of 800 cm^{-1} were exchanged preferentially while the bands at around 900 cm^{-1} were affected very little. The reoxidation seemed to take place at the vacancies corresponding to the oxygen atoms whose bands shifted preferentially. This spectroscopic approach for studying oxygen exchange in Bi–Mo and Mo mixed oxide catalysts has several other precedents (11, 15–17).

The oxidation of stereolabeled propene to acrolein has been studied by one author (R.L.K.) over Bi–Mo oxides (18), Cu_2O (18, 19), and Rh catalysts (18). With Bi_2MoO_6 and $Bi_2Mo_2O_9$ catalysts (18), a deuterium isotope effect in the second hydrogen abstraction as observed by Grasselli *et al.* (1, 36) was confirmed, as well as their suggestion of a rapid conversion between π-allyl and σ-allyl intermediates. The oxidation of cis-CHD=CD–CH_3 propene over mixed Sb oxide catalysts (20, 21) did not exhibit a marked isotope effect for the second hydrogen abstraction. The absence of an isotope effect was similar to oxidations over a Rh catalyst. Complete stereo randomization about the double bond occurred in the product except for the Rh catalyst.

In this work, the lattice oxygen atoms of an α-$Bi_2Mo_3O_{12}$ catalyst were exchanged in the oxidations of propene and trans-2-butene using $^{18}O_2$. Laser Raman spectra of the α-phase were obtained and compared with an unexchanged catalyst. The characteristic features of the Raman band shifts in the spectra between 800 and 1000 cm^{-1} were compared and discussed. A correlation between the Raman band position and the Mo–O species was made using the

[1] To whom correspondence should be addressed. E-mail: ono@chem.osakafu-u.ac.jp.
[2] Present address: Teijin Kakoshi Co. Ltd, Komatsu, Fukui, Japan.

0021-9517/98 $25.00

diatomic approximation. The preferential exchange of certain Mo–O bonds in these olefin oxidations was proposed. The oxidation of labeled propene cis-CHD=CD–CH_3 was carried out over supported and unsupported α-$Bi_2Mo_3O_{12}$ and MoO_3 catalysts. The deuterated acrolein ratios and the isotope effect of the second hydrogen abstraction were determined. The results were compared with those for other catalysts. The oxidation intermediates and mechanism of olefin oxidation over α-$Bi_2Mo_3O_{12}$ were discussed on the basis of these Raman and microwave results.

2. METHODS

2.1. Catalysts

Both α-$Bi_2Mo_3O_{12}$ supported and unsupported catalysts were used. The α-$Bi_2Mo_3O_{12}$ supported on ZrO_2 (15 atom%) was prepared as follows: a nitric acid solution of $Bi(NO_3)_3 \cdot 5H_2O$ was first impregnated on ZrO_2, then dried and heated at 723 K. Mo oxide was added next using an ammonium heptamolybdate solution. After evaporation over a water bath, the catalyst was heated at 723 K for 10 h. The unsupported α-$Bi_2Mo_3O_{12}$ was prepared from $Bi(NO_3)_3 \cdot 5H_2O$ and ammonium heptamolybdate by heating at 723 K. The unsupported MoO_3 catalyst was prepared by heating ammonium heptamolybdate at 723 K.

2.2. Procedures

The catalyst structure was determined by X-ray diffraction using CuKα radiation and a Rigaku Denki Rad-rA diffractometer. The particle size was determined by a line broadening method using well-crystallized quartz.

The catalytic oxidation of olefins and the oxygen exchange of the catalysts were carried out using a mixture of the olefin at 2.7 kPa and $^{18}O_2$ (Isotec Inc., 98%) at 2.7 kPa over the α-$Bi_2Mo_3O_{12}$ catalysts at 673–723 K in a circulation system (ca 300 cm^3). In the case of the oxidation of propene, the amounts of product such as acrolein (ca 90%) and CO_2 (ca 10%) were determined by gas chromatography. The ^{18}O% in the products was determined by mass spectroscopy. The average exchange percentage in the α-$Bi_2Mo_3O_{12}$ catalyst was estimated by assuming that the amount of ^{16}O in the products was the same as that exchanged with ^{18}O in the catalysts. Details with propene are also discussed in Section 3.4. In the case of trans-but-2-ene, the amount of buta-1, 3-diene produced (>90%) was determined by GC and the ^{18}O% in H_2O was determined by mass spectroscopy. The average ^{18}O% exchange in the catalysts after the oxidation was discussed since it was important where the reaction took place.

Raman spectra of the catalysts exchanged with ^{18}O were recorded on a JASCO NR-1000 laser Raman spectrometer (Osaka Prefecture University). An Ar-ion laser was tuned to the 514.5 nm line for excitation. The laser power was set at 150–200 mW. The data were stored on a computer and a band-shape analysis was carried out using the technique reported by Miyata *et al.* (22, 23).

The catalytic oxidation of cis-CHD=CD–CH_3 (MSD Canada, Ltd, 96.7%) was carried out in a closed circulation system (ca 1000 cm^3) over α-$Bi_2Mo_3O_{12}$ and MoO_3 catalysts. During the reaction, the products such as acrolein and H_2O were trapped at ethanol slush temperature (ca 173–163 K). The acrolein, acetaldehyde, and CO_2 were analyzed by gas chromatography. Microwave spectroscopy was used to determine the relative amounts of the isotopic acrolein products using a Hewlett-Packard 8460A spectrometer (18–21). Three to five sets of rotational transitions were compared and the peak intensities were converted into molar ratios. Mainly the 4_{04}-3_{03}, 4_{14}-3_{13}, and 4_{13}-3_{12} transitions were used. The precision in the isotopic ratios (5 to 10%) is sufficient to provide useful insights on the reaction processes.

3. RESULTS AND DISCUSSION

3.1. Characterization of Catalysts

The properties of the catalysts used are shown in Table 1. The characterization of the 15 atom% Bi–Mo(2/3)/ZrO_2 catalyst was carried out by X-ray diffraction and laser Raman spectroscopy as reported in a previous paper (14). The fraction of crystalline α-$Bi_2Mo_3O_{12}$ was determined by a comparison of diffraction intensities and peak intensities of the catalysts with a mechanical mixture of α-$Bi_2Mo_3O_{12}$ and ZrO_2. The fraction of α-phase was obtained as 30–40% (Table 1). Generally, the Raman intensity was very strong for the crystalline compounds while the dispersed and noncrystalline compounds exhibited little or no intensity (24). As shown in Fig. 1a, the 15 atom% Bi–Mo(2/3)/ZrO_2 catalyst exhibited six bands at 1000–800 cm^{-1} originating from the crystalline α-$Bi_2Mo_3O_{12}$ phase (14, 27) and some bands at 600–480 cm^{-1} from crystalline ZrO_2. The noncrystalline Bi–Mo oxides should be present on ZrO_2 or may be

TABLE 1

Properties of the Catalysts

Catalyst	Crystal phase	Surface area/ $m^2\ g^{-1}$	Percentage crystalline	
			X-ray	Raman
Bi–Mo(2/3)/ZrO_2 15 atom% supported	α-$Bi_2Mo_3O_{12}$	42	44	32
Bi–Mo(2/3) unsupported	α-$Bi_2Mo_3O_{12}$	1–2		
Mo oxide unsupported	MoO_3	2		

Note. The average particle size of α-$Bi_2Mo_3O_{12}$ on Bi–Mo(2/3)/ZrO_2 was ca 1600 Å. Those of unsupported α-$Bi_2Mo_3O_{12}$ and MoO_3 were >5000 Å.

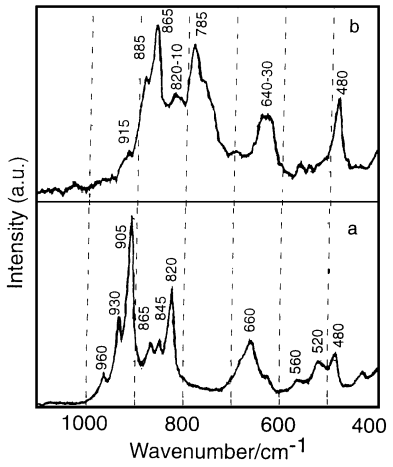

FIG. 1. Laser Raman spectra of α-$Bi_2Mo_3O_{12}/ZrO_2$ before and after exchange with ^{18}O: (a) no exchange; (b) reduction by but-1-ene and reoxidation by $^{18}O_2$ were repeated 10 times at 700 K (one time, ca 25–30 μmol of ^{18}O was replaced in 0.05 g of catalyst). All oxygen ions seem to be replaced with ^{18}O. The selectivities to buta-1,3-diene were ca 90%. The spectra in the range from 400 to 630 cm^{-1} contain bands of ZrO_2.

sandwiched between the α-$Bi_2Mo_3O_{12}$ and ZrO_2 phases. The ZrO_2 surface also was exposed since its Raman bands were observed.

3.2. Band Shifts in the Raman Spectra of α-$Bi_2Mo_3O_{12}$ Exchanged with ^{18}O

In order to analyze the spectral shifts for α-$Bi_2Mo_3O_{12}$ exchanged with ^{18}O, the α-$Bi_2Mo_3O_{12}/ZrO_2$ catalyst was reduced with but-1-ene and reoxided by $^{18}O_2$ repeatedly. Figure 1a is the original spectra before exchange. Figure 1b shows the spectra after being highly exchanged. These results suggest that the bands at 960, 930, 905, 865, 845, and 820 cm^{-1} shift to 915, 885, 870, 820–810, and 785 cm^{-1}. Similar results were also reported previously (14). The theoretical shifts using a Mo–O diatomic stretching model are calculated as 45–40 cm^{-1} in the 900–800 cm^{-1} regions. The observed values are 45–35 cm^{-1}, which are nearly the same as those calculated.

3.3. Crystal Structure and Raman Band Assignment for α-$Bi_2Mo_3O_{12}$

Figure 2 shows the structure of α-$Bi_2Mo_3O_{12}$ reported by Cesari *et al.* (25). It consists of two kinds of twin tetrahedra, i.e. $\alpha_1\alpha_1$ and $\alpha_2\alpha_3$. Thus, three kinds of tetrahedra are present, α_1, α_2, and α_3. As seen in Fig. 2, α_1 and α_2 have Bi ions adjacent to the tetrahedra, while there is a Bi ion vacancy near the α_3 tetrahedron. Elzen *et al.* (26) have reported the structure and Mo–O distances of each tetrahedron. Matsuura *et al.* (27) reported that the bands around 900 and 800 cm^{-1} can be attributed to the stretching modes of each tetrahedral species incorporating the Cotton–Wing relation (28) into a FG analysis of the modes, i.e., 960 cm^{-1} (1.68A, α_3), 930 (1.69A, α_1), 905 (1.72A, α_2), 865 (1.72A, α_1), 845 (1.73A, α_2), and 820 (1.78A, α_3) as shown in Table 4. Using the correlation between Raman bands and Mo–O distances for the α-phase as proposed by Hardcastle and Wachs (29), the assignments for the Mo–O species are the same as those by Matsuura *et al.* (27). We also made some modifications to Hardcastle's previously reported data (14). The Cotton–Wing relations, the report by Matsuura *et al.*, and those by Hardcastle *et al.* are based on a diatomic approximation. For the bands in the α-phase in the range 1000–800 cm^{-1} exchanged with ^{18}O, experimental shifts of 45–35 cm^{-1} were obtained in this work, suggesting that the diatomic approximation is applicable in this range.

3.4. Catalytic Oxidation and Oxygen Exchange Using $^{18}O_2$ over α-$Bi_2Mo_3O_{12}$

Oxygen exchange of the 15 atom% α-$Bi_2Mo_3O_{12}/ZrO_2$ via catalytic olefin oxidation using $^{18}O_2$ was carried out. The acrolein selectivity in the oxidation of propene is ca 80–90% and the CO_2 selectivity is below 20% as shown in Table 2. The ^{18}O% in acrolein and CO_2 are 60–70% and 20%, respectively. According to previous work (30) over mixed Mo oxide catalysts, the ^{18}O% in the acrolein and CO_2 were almost the same while the results in this work show a large difference. The selectivity to acrolein on α-$Bi_2Mo_3O_{12}$ was generally reported as more than 90% in the past (7). Acrolein molecules will be formed mainly on the crystalline α-$Bi_2Mo_3O_{12}$. H_2O and CO_2 also will be formed on this surface and on the ZrO_2. It seems difficult to determine the true percentage exchange with ^{18}O on this supported catalyst. Assuming that the acrolein and an equimolar amount of H_2O are produced on the Bi–Mo oxides (crystalline

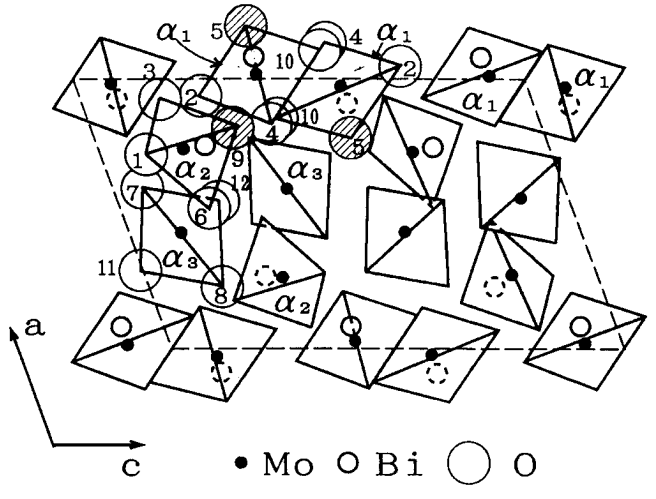

FIG. 2. Projection along the b axis of the structure of α-$Bi_2Mo_3O_{12}$ reported by Cesari *et al.* (25) and Elzen *et al.* (26). α_1, α_2, and α_3 denote Mo tetrahedra. The numerals denote the oxygen position numbers reported by Elzen *et al.* The shaded oxygen circles denote the well-exchanged positions in text. (Note: the numbering of Mo(2) and (3) are reversed in the $\alpha_2\alpha_3$ twin tetrahedra in Fig. 2 of Ref. (26)).

TABLE 2

Material Balance in Propene Oxidation over α-$Bi_2Mo_3O_{12}/ZrO_2$ with $^{18}O_2$ p(C_3H_6) = 20 Torr, p($^{18}O_2$) = 20 Torr (1 Torr = 133.3 Pa), temp. 673 K, and cat. 0.03 g

Reaction time/min	15	50
Acrolein formed/μmol	24	59
Selectivity/%	89	82
^{18}O% in acrolein	62	65
CO_2 formed/μmol	9.1	40
^{18}O% in CO_2	20	<20
Average exchange%[a]	ca 25	ca 50

[a] Average exchange % is estimated using the amount of oxygen-16 in (CH_2=CH−CHO + H_2O) and ca 80 μmol of oxygen (see text) in 0.03 g of $Bi_2Mo_3O_{12}/ZrO_2$ (15 atom%).

α-phase + noncrystalline), the percentage exchange for the Bi–Mo oxides is estimated as in Table 2. With trans-but-2-ene, the selectivity to buta-1,3-diene is above 90% as shown in the Table 3. The percentage exchange for the Bi–Mo oxides (crystalline α-phase + noncrystalline phase) was calculated using the ^{18}O% in H_2O. The secondary exchange of H_2 ^{18}O with surface OH groups can not be excluded. Thus, the average ^{18}O percentage on crystalline α-$Bi_2Mo_3O_{12}$ are roughly estimated as in Table 3.

3.5. Raman Spectra and Peak-Shape Analysis of α-$Bi_2Mo_3O_{12}/ZrO_2$ Exchanged with ^{18}O Tracer via Propene Oxidation

Figures 3a and 4a show the Raman spectra after ^{18}O exchange via propene oxidation as noted in Table 2. The band at 845 cm^{-1} has decreased as the ^{18}O content increased. A weak new peak at 785 cm^{-1} has appeared. These results were reported previously (14). In this work, a peak-shape analysis was carried out for the six peaks. In this analysis, the following ratios for the original spectra (Fig. 1a) were used as the base; $I_{960} : I_{945} : I_{905} = 0.11 : 0.38 : 1.0$ and $I_{865} : I_{845} : I_{820} = 1.0 : 1.0 : 3.0$, where I denotes the area determined by the peak shape analysis. The summed Lorentzian

TABLE 3

Material Balance in Trans-but-2-ene Oxidation over α-$Bi_2Mo_3O_{12}/ZrO_2$ with $^{18}O_2$

Reactant: trans-but-2-ene Reaction time/min	15	50
But-1,3-diene formed/μmol	38	75
Selectivity/%	95	93
^{18}O% in H_2O	52	ca 50
Average exchange%[a]	25	47

Note. p(butene) = 20 Torr, p($^{18}O_2$) = 20 Torr, temp. 673 K, and cat. 0.03 g.

[a] Average exchange % was calculated using the amount of oxygen-16 in H_2O and ca 80 μmol of oxygen (see text) in 0.03 g of $Bi_2Mo_3O_{12}/ZrO_2$ (15 atom%).

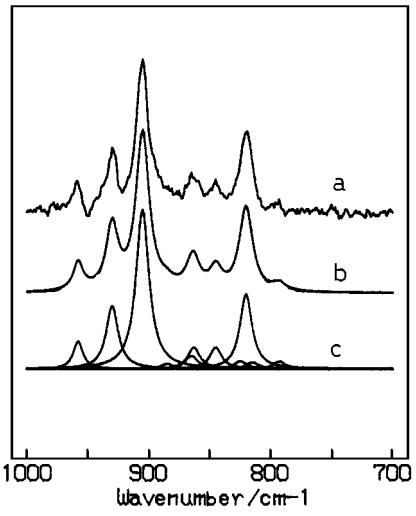

FIG. 3. Raman spectra of α-$Bi_2Mo_3O_{12}/ZrO_2$ exchanged with ^{18}O via propene oxidation and band shape analysis. The bands at 960, 930, 905, 865, 845, and 820 cm^{-1} and the shifted bands at 890–885, 863, 820, 815–810, and 790–785 cm^{-1} were used: (a) original spectra exchanged by an average of 25% (see Table 2); (b) summed spectra; (c) separated peaks.

curves (Figs. 3b and 3c) were fitted to the experimental spectrum (Fig. 3a) by trial and error. The separated peak positions which are shown in the caption of Fig. 3 were determined experimentally as shown in Fig. 1. For example, with the bands in the 800 cm^{-1} region, the intensity decreases in the 865, 845, and 820 cm^{-1} bands are linked with the increases in the bands at 820, 810, and 785 cm^{-1}. The ratio $(I_{865} + I'_{820}) : (I_{845} + I_{810}) : (I_{820} + I_{785})$ is adjusted as ca 1 : 1 : 3 during fitting, where I'_{820} and I_{820} are distinct in the analysis. With the bands in the 900 cm^{-1} region, the intensity decreases in the 930 and 905 cm^{-1} bands are linked

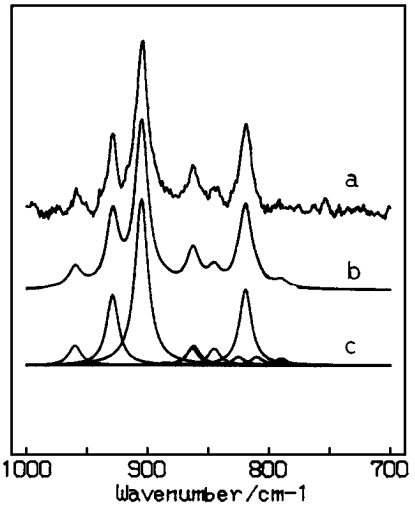

FIG. 4. Raman spectra of α-$Bi_2Mo_3O_{12}/ZrO_2$ exchanged with ^{18}O via propene oxidation and peak-shape analysis. The bands used were nearly the same as Fig. 3: (a) original spectra exchanged by an average of 50% (see Table 2); (b) summed spectra; (c) separated peaks.

TABLE 4

Band Shift Fractions for α-$Bi_2Mo_3O_{12}/ZrO_2$ Exchanged with ^{18}O

Mo–O species	Mo(3)–O(12)	Mo(1)–O(4)	Mo(2)–O(1)
Band/cm^{-1}	960(α_3)	930(α_1)	905(α_2)
Fraction shifted	[a]	$I_{885}/(I_{930}+I_{885})$	$I_{865}/(I_{905}+I_{865})$
Olefin (average exchange%)			
C_3H_6 (25%)		0.08	0.08
(50%)		0.04	0.10
trans-2-C_4H_8 (25%)		0.08	0.06
(47%)		0.3	0.1
Mo–O species	Mo(1)–O(5)	Mo(2)–O(9)	Mo(3)–O(11)
Band/cm^{-1}	865(α_1)	845(α_2)	820(α_3)
Fraction shifted	$I_{820}/(I_{865}+I_{820})$	$I_{810}/(I_{845}+I_{810})$	$I_{785}/(I_{820}+I_{785})$
Olefin (average exchange%)			
C_3H_6 (25%)	0.27	0.24	0.09
(50%)	0.33	0.33	0.09
trans-2-C_4H_8 (25%)	0.26	0.28	0.13
(47%)	0.25	0.25	0.23

[a] Analysis of the 960 cm^{-1} band was not attempted since its exchange was low.

with the increases in the bands at 890 and 865 cm^{-1}. The 915 cm^{-1} peak which shifted from the 960 cm^{-1} band is omitted here since this data seemed to be less useful. The ratio $I_{960}:(I_{930}+I_{890}):(I_{905}+I_{865})$ is maintained as 0.10–0.12 : 0.38 : 1.0 which is also nearly the same as the original spectra ratio. The analysis was made for two or three spectra for a catalyst sample. The reproducibility was about 20–30%.

The relative fractions for each band are shown in the Table 4. The shape analysis suggests that the bands at 865 as well as 845 cm^{-1} are exchanged preferentially and other bands are less affected. In our previous work, (14) the analysis was made on the assumption of no shift of the 820 cm^{-1} band since the band intensity at 865 cm^{-1} was unclear. In this work, a decrease in the 865 cm^{-1} band and a small shift contribution from 905 cm^{-1} were observed as described above.

3.6. Raman Spectra and Peak-Shape Analysis of α-$Bi_2Mo_3O_{12}/ZrO_2$ Exchanged with ^{18}O Tracer via Trans-but-2-ene Oxidation

Figures 5a and 6a show the Raman spectra exchanged with ^{18}O in the oxidation of trans-but-2-ene as noted in Table 3. In this case, the band at 845 cm^{-1} decreased and a new peak at 785 cm^{-1} appears. In order to investigate the changes in detail, a peak-shape analysis was also carried out with the results in Figs. 5a and 6a. The analysis was made the same as in the oxidation of propene. The results in Table 4 indicate that the bands at 865 and 845 cm^{-1} are exchanged preferentially in the 25% exchanged sample. This is the same tendency as for propene. However, the results at long reaction times are somewhat different. Some difference might be expected due to the absence of oxygen vacancies being generated by conversion of an allyl species to acrolein.

3.7. Reoxidation Sites for α-$Bi_2Mo_3O_{12}$

In the oxidation of propene, the bands at 865 and 845 cm^{-1} are preferentially exchanged. This suggests that the oxygen atoms are mainly inserted at the vacancies corresponding to Mo(1)–O(5) bonds (1.72A) in the α_1 tetrahedron and Mo(2)–O(9) bonds (1.73A) in the α_2 tetrahedron

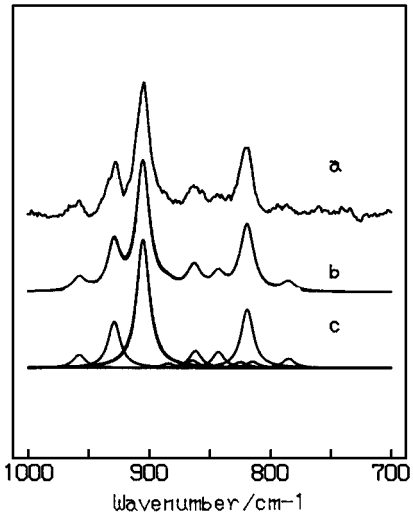

FIG. 5. Raman spectra of α-$Bi_2Mo_3O_{12}/ZrO_2$ exchanged with ^{18}O via trans-but-2-ene oxidation and peak-shape analysis. The bands at 960, 930, 905, 865, 845, and 820 cm^{-1} and the shifted bands at 885, 865, 820, 815–810, and 785 cm^{-1} were used: (a) original spectra exchanged by an average of 25% (see Table 3); (b) summed spectra; (c) separated peaks.

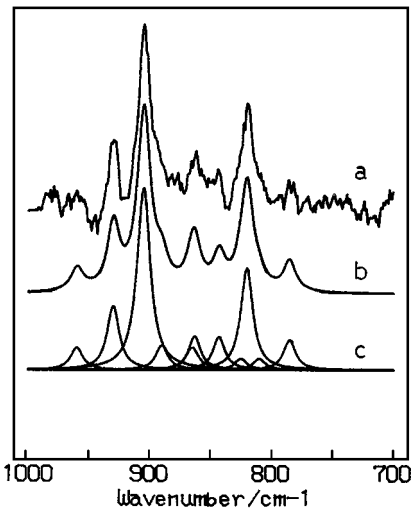

FIG. 6. Raman spectra of α-$Bi_2Mo_3O_{12}$/ZrO_2 exchanged with ^{18}O via trans-but-2-ene oxidation and peak-shape analysis. The bands used were nearly the same as Fig. 5: (a) original spectra exchanged by an average of 47% (see Table 3); (b) summed spectra; (c) separated peaks.

in accordance with Table 4 and Section 3.3. The band at 820 cm^{-1} attributed to the α_3 tetrahedron is affected less than these bands. The bands at 960–905 cm^{-1} did not exchange as much. This suggests that the Mo(1)–O(4) bond (1.69A) in α_1, Mo(2)–O(1) (1.72A) in α_2, and Mo(3)–O(12) (1.68A) in α_3, which are the strongest bonds in each Mo tetrahedron, do not react very much and are not related to reoxidation. The α_1 and α_2 sites are more active than α_3 for oxidation reactions. The lesser activity of the α_3 sites seems to be related to the Bi ion vacancies near α_3. In the oxidation of trans-but-2-ene, preferential exchange at 865 and 845 cm^{-1} was found initially as for propene oxidation. This also suggests that the anion vacancies corresponding to Mo(1)–O(5) in α_1 and Mo(2)–O(9) in α_2 are involved in reoxidation. As reported previously (13, 14), upon reduction with but-1-ene and reoxidation with $^{18}O_2$ separately, preferential exchange was found for the bands at 865 and 845 cm^{-1} and reoxidation took place on these anion vacancies selectively.

According to Elzen *et al.* (26), the four Mo–O distances in the α_1 tetrahedron (Figs. 2 and 7) are 1.69A for O(4), 1.72A for O(5), 1.85A for O(2), and 1.91A for O(10). The difference in exchange activity between the O(4) and O(5) oxygen positions presumably originates from association with the allyl intermediate and reoxidation after oxygen release. Less information is available on the O(2) and O(10) oxygen species and their role is unclear at present. The same situation is expected for the α_2 tetrahedron.

3.8. Deuterium Labeled Propene Oxidation over α-$Bi_2Mo_3O_{12}$ and MoO_3

It is well known that hydrogen abstraction from the methyl group is the rate determining step in the oxidation of propene over various catalysts (31–34, 20) including α-$Bi_2Mo_3O_{12}$ (35, 36). In order to probe whether any subtle stereochemical effect may be transferred through the first and second hydrogen abstraction step, the oxidation of cis-CHD=CD–CH_3 was studied over α-$Bi_2Mo_3O_{12}$ and MoO_3 catalysts. The reaction conditions for oxidation are shown in

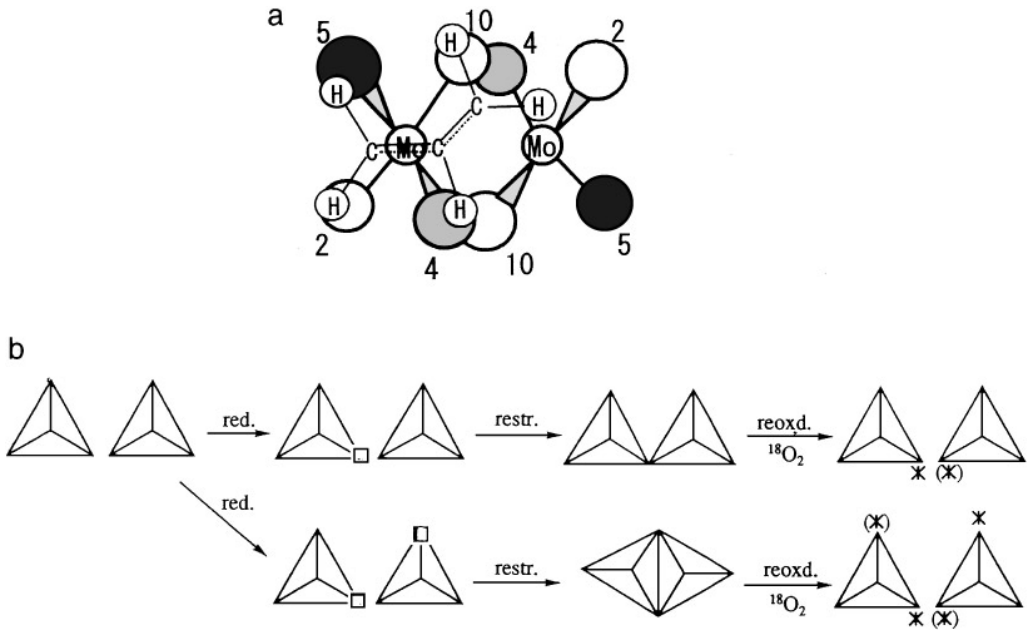

FIG. 7. (a) Possible oxygen species and π- or σ-allyl species on the α_1 tetrahedron. The darkly shaded circle denotes the well-exchanged positions. The lightly shaded circle denotes the unexchanged positions. Numerals on oxygen denote the oxygen position number reported by Elzen *et al.* (26). (b) A mechanism for vacancy formation, restructuring, and reoxidation of twin $\alpha_1\alpha_1$ Mo tetrahedra at the surface (adopted from Ref. (40)).

TABLE 5

Relative Acrolein Formation Rates from the Oxidation of cis-CHD=CD–CH_3 over α-$Bi_2Mo_3O_{12}$ Catalysts

	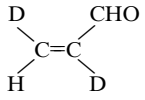 (ACR-trans-2,3-d_2)	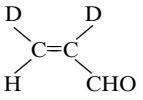 (ACR-cis-2,3-d_2)	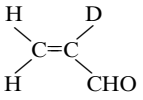 (ACR-2-d_1)	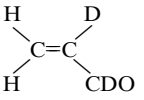 (ACR-1,2-d_2)
$Bi_2Mo_3O_{12}$[a]	1.00	0.98	0.57	0.92
$Bi_2Mo_3O_{12}/ZrO_2$[b]	1.00	0.98	0.77	1.05

[a] Unsupported catalyst in Table 1, p(propene) = 8 Torr, $p(O_2)$ = 25 Torr, temp. 673 K, cat. 0.5 g, and reaction time 30 min.
[b] Supported catalyst in Table 1, p(propene) = 14 Torr, $p(O_2)$ = 30 Torr, temp. 673 K, cat. 0.1 g, and reaction time 30 min.

the notes of Tables 5 and 6. The rates of cis-CHD=CD–CH_3 conversion at 673 K over the catalysts in Table 1 were as follows: 0.4 μmol/m^2 min over unsupported α-$Bi_2Mo_3O_{12}$, ca 2 over $Bi_2Mo_3O_{12}/ZrO_2$, and 1–2 over MoO_3. The selectivities to acrolein over the supported and unsupported α-phase catalysts were ca 80–90%. The selectivities to acrolein and acetaldehyde over MoO_3 were 20–35 and 20%, respectively. Acetaldehyde seems to be formed via a different path of allylic oxidation (38).

The formation of a π-allyl intermediate (CHD–CD–CH_2) should lead to four propenal (acrolein) species as shown scheme.

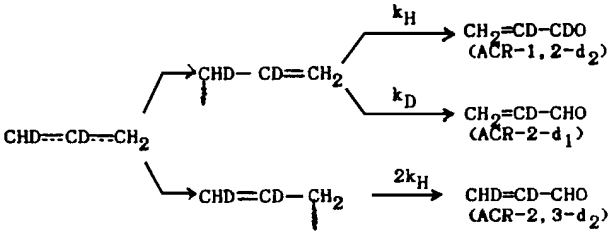

The experimental results for the four species over α-$Bi_2Mo_3O_{12}$ and MoO_3 are shown in Tables 5 and 6. For α-$Bi_2Mo_3O_{12}$ in Table 5, the ratio ACR-2-d_1 : ACR-1,2-d_2 : cis-ACR-2,3-d_2 : trans-ACR-2,3-d_2 is 0.57 : 1 : 1 : 1 for the unsupported catalyst and 0.77 : 1 : 1 : 1 for the supported catalyst. It was shown in previous work (18–20) that the ratio depends on the catalyst. With a Bi–Mo oxide catalyst such as the γ-phase, the ratio should be approximately 0.5 : 1 : 1 : 1 since the terminal hydrogen and deuterium atoms of the allyl species have an equal probability of abstraction except for a deuterium isotope effect and product stereo randomization is known to occur with this phase and the β-phase (18). This implies a fast equilibration between π-allyl and σ-allyl intermediates. In this work, the ratios are 0.57 : 1 : 1 : 1 for the unsupported α-phase and 0.77 : 1 : 1 : 1 for the supported α-phase, indicating that a rapid equilibration and stereo randomization has occurred. In the case of the supported catalyst, the isomerization of cis-CHD=CD–CH_3 also took place and ca 30% of CH_2D–CD=CH_2 was detected after reaction for 1 h as well as the trans- isomer. The CH_2D–CD=CH_2 species brings about the increase in the amount of ACR-2-d_1. The result for the supported catalyst in Table 5 is obtained after reaction for 30 min. The influence of isomerization seems to be less significant in the reaction time for 0–30 min. The prospect of allyl alcohol and propene isomerization processes in acrolein production on acid sites over α-phase (and over MoO_3; see below) has been discussed previously (36).

TABLE 6

Relative Acrolein Formation Rates from the Oxidation of cis-CHD=CD–CH_3 over MoO_3 as a Function of Reaction Time

Reactions conditions	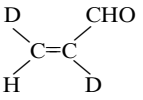 (ACR-trans-2,3-d_2)	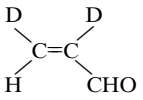 (ACR-cis-2,3-d_2)	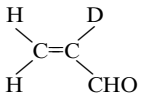 (ACR-2-d_1)	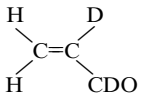 (ACR-1,2-d_2)
A	1.00	0.96	0.85	1.07
B	1.00	1.03	1.04	1.06
C	1.00	1.00	1.50	1.00

Note. A, acrolein produced at p(propene) = 14 Torr, $p(O_2)$ = 25 Torr, temp. 673 K, cat. 0.30 g, and reaction time 30 min. B, acrolein produced for another 20 min soon after A. C, the same conditions as A for 65 min of reaction time.

TABLE 7

Relative Amounts of Acrolein Obtained from the Oxidation of CH_2=CH–CH_3 and CH_2=CH–CD_3 (1 : 1) over a MoO_3 Catalyst

	CH_2=CH–CHO	CH_2=CH–CDO	CD_2=CH–CHO
Ratio	1.00	0.16	0.24

Note. CH_2=CH–CH_3 = 8 Torr, CH_2=CH–CD_3 = 8 Torr, O_2 = 30 Torr, temp. 673K, MoO_3 1 g, and reaction time 2 h.

The results with the MoO_3 catalyst are shown in Table 6. The ratio ACR-2-d_1 : ACR-1,2-d_2 : cis-ACR-2,3-d_2 : trans-ACR-2,3-d_2 equals 0.85 : 1 : 1 : 1 for a reaction time of 30 min. It changes to 1.5 : 1 : 1 : 1 after 65 min. This ratio change should not be caused by a secondary exchange of acrolein with the catalyst surface since the acrolein was trapped at ca 163 K after production. The change again seems to originate from the isomerization of cis-CHD=CD–CH_3 on the surface. Kondo *et al.* (37) have reported on the intermediates likely upon exchange of propene. If a 2-propyl mechanism occurs via H^+ addition to the terminal carbon and release of H^+ or D^+, species such as CH_3–CD=CH_2 increase, which will bring about an increase in the ACR-2-d_1 species. The surface on MoO_3 seems to show an increase in H^+ acidity probably due to adsorbed H_2O at longer reaction times. In the initial stage of reaction, however, the ratio seems to be 0.6 : 1 : 1 : 1 when the amount of H_2O will be small. MoO_3 is known as a more acidic catalyst than α-$Bi_2Mo_3O_{12}$ (36). In this case, it appears that unsupported α-$Bi_2Mo_3O_{12}$ catalyst exhibits low acidity even in the presence of water.

3.9. Oxidation of Equimolar Mixture of CH_2=CH–CH_3 and CH_2=CH–CD_3 over MoO_3

Table 7 shows the results upon the oxidation of an equimolar mixture of CH_2=CH–CH_3 and CH_2=CH–CD_3. The ratio CH_2=CH–CHO/(CH_2=CH–CDO + CD_2=CH–CHO) is 1/0.4, which corresponds to the first deuterium isotope effect for acrolein formation. The ratio of CH_2=CH–CDO/CD_2=CH–CHO is 0.6/1.0, which corresponds to the second deuterium isotope effect from the allyl species. These results indicate that isotope effects for the first and second hydrogen abstraction take place on MoO_3. The isomerization of the deuterated olefin also occurred over the MoO_3 catalyst as described above. However, CD_2=CH–CH_3 will be mainly formed from the reactant CH_2=CH–CD_3 by a 2-propyl mechanism (37). This may not affect the acrolein ratios since the hydrogen abstraction from CD_2=CH–CH_3 produces the same allyl species as from CH_2=CH–CD_3. Portefaix *et al.* (38) found no isotope effect for acrolein formation in the oxidation of CD_2=CH–CH_3 over a MoO_3/SiO_2 catalyst. The origin of the difference in this work is unclear. It may arise from a catalyst support interaction which inhibits rapid σ-π allyl equilibration.

Thus, it is concluded that the ratio ACR-2-d_1 : ACR-1,2-d_2 : cis-ACR-2,3-d_2 : trans-ACR-2,3-d_2 is 0.6 : 1 : 1 : 1 for unsupported and supported α-$Bi_2Mo_3O_{12}$ and MoO_3 catalysts if the isomerization of deuterated propene is absent. This also suggests that a rapid equilibration between the π-allyl and σ-allyl intermediates takes place on α-$Bi_2Mo_3O_{12}$, i.e., on the Mo tetrahedra, in agreement with the Grasselli–Burrington mechanism (1–6).

4. CONCLUSION

As described in the Introduction, previous work (1–6) revealed that the initial hydrogen abstraction involves an oxygen atom associated with bismuth atoms and that the second hydrogen abstraction is facilitated by the presence of molybdenum-oxygen polyhedra. In this work, the results for the deuterated propene oxidation confirm earlier studies (1–6, 36), that a rapid equilibration between π-allyl and σ-allyl occurs on the Mo ions of α-$Bi_2Mo_3O_{12}$. The laser Raman results indicate that the α_1 and α_2 Mo tetrahedra where Bi cations are present seem to be more active, indicating the importance of the presence of Bi ions on the molecular scale. The π- or σ-allyl intermediates of propene on the α_1 Mo tetrahedron are shown as in the Fig. 7a. The possible participation of the O(5) and O(10) oxygen atoms with an allyl species is shown. Other sets such as O(5)–O(2) and O(2)–O(10) are possible while the O(4) in the O–O sets is excluded here since it had a low ^{18}O exchange activity. Anderson *et al.* (39) have studied the formation of acrolein using molecular orbital theory on a surface cluster model of α-$Bi_2Mo_3O_{12}$. The C–C, C–H, and Mo–O lengths, coordination etc. may change along the oxidation steps as they suggested. Such details are unclear here. After acrolein formation, the twin $\alpha_1\alpha_1$ tetrahedra where vacancies were produced may be restructured to corner or edge linked tetrahedra as shown in Fig. 7b. When they return to the original $\alpha_1\alpha_1$ by reoxidation, the preferential insertion of ^{18}O should take place on sites such as O(5) and O(10). A similar reconstruction mechanism was reported by Brazdil *et al.* (40). A similar mechanism should take place for the $\alpha_2\alpha_3$ tetrahedra although the oxygen in α_3 is less active. In the oxidation of trans-but-2-ene, the second hydrogen abstraction is likely somewhat different compared to the case of propene. The difference in ^{18}O exchange features at long reaction times seems to correlate with this difference.

ACKNOWLEDGMENTS

We thank Professor H. Miyata of Hiroshima Prefecture University for his help with the band shape analysis by computer. The microwave spectrometer at the University of Michigan was supported by a grant from the National Science Foundation, Washington, DC.

REFERENCES

1. Grasselli, R. K., Burrington, J. D., and Brazdil, J. F., *Faraday Disc. Chem. Soc.* **72**, 203 (1982).
2. Burrington, J. D., Kartisek, C. T., and Grasselli, R. K., *J. Catal.* **81**, 489 (1983).
3. Grasselli, R. K., and Burrington, J. D., *I & E Product Res. Dev.* **23**, 393 (1984).
4. Grasselli, R. K., Brazdil, J. F., and Burrington, J. D., *Proc. 8th Int. Congr. Catal.*, Berlin, V, 369 (1984).
5. Grasselli, R. K., *J. Chem. Ed.* **63**, 216 (1986).
6. Grasselli, R. K., and Burrington, J. D., *Adv. Catal.* **30**, 133 (1981).
7. Snyder, T. D., and Hill, G. C. J., *Catal. Rev. Sci. Eng.* **31**, 43 (1989).
8. Otubo, T., Miura, H., Morikawa, Y., and Shirasaki, T., *J. Catal.* **36**, 240 (1975); Miura, H., Otubo, T., Shirasaki, T., and Morikawa, Y., *J. Catal.* **56**, 84 (1979).
9. Gryzbowska, B., Haber, J., and Janas, J., *J. Catal.* **49**, 150 (1977); Bruckman, K., Haber, J., and Wiltowski, T., *J. Catal.* **106**, 188 (1987).
10. Grasselli, R. K., *Appl. Catal.* **15**, 127 (1985).
11. Glaeser, I. C., Brazdil, J. F., Hazle, M. A., and Grasselli, R. K., *J. Chem. Soc. Faraday Trans. I* **81**, 2903 (1985).
12. Ono, T., Numata, H., and Ogata, N., *J. Mol. Catal. A: Chemical* **105**, 31 (1996).
13. Ono, T., Ogata, N., and Miyaryo, Y., *J. Catal.* **161**, 78 (1996).
14. Ono, T., and Ogata, N., *J. Chem. Soc. Faraday Trans.* **90**, 2113 (1994).
15. Hoefs, E. V., Monnier, J. V., and Keulks, G. W., *J. Catal.* **57**, 331 (1971).
16. Matsuura, I., Hashiba, H., and Kanesaka, I., *Chem. Lett.*, 533 (1986). [Kanesaka, I., Kirishiki, M., and Matsuura, I., *J. Raman Spectros.* **23**, 201 (1992).]
17. Ozkan, U. S., Smith, M. R., and Driscoll, S. A., *J. Catal.* **134**, 24 (1992).
18. Imachi, M., Kuczkowski, R. L., Groves, J. T., and Cant, N. W., *J. Catal.* **82**, 355 (1983).
19. Choi, H., Lin, J., and Kuczkowski, R. L., *J. Catal.* **99**, 72 (1986).
20. Ono, T., Hillig II, K. W., and Kuczkowski, R. L., *J. Catal.* **123**, 236 (1990).
21. Ono, T., Kiryu, M., Komiyama, M., and Kuczkowski, R. L., *J. Catal.* **127**, 698 (1991).
22. Miyata, H., Fujii, K., Inui, S., and Kubokawa, Y., *Appl. Spectrosc.* **40**, 1177 (1986).
23. Miyata, H., Tokuda, S., and Yoshida, T., *Appl. Spectrosc.* **43**, 522 (1989).
24. Roozeboom, F. R., Medema, J., and Gellings, P. J., *Z. Phys. Chem. N. F.* **111**, 215 (1978); Ono, T., Miyata, H., and Kubokawa, Y., *J. Catal.* **62**, 26 (1980).
25. Cesari, M., Pergo, G., Zazetta, A., Manara, G., and Notari, B., *Inorg. Nucl. Chem.* **33**, 3595 (1971).
26. Elzen, A. F. V., and Rieck, G. D., *Acta. Crystallogr. Sect. B* **29**, 2433 (1973).
27. Matsuura, I., Shut, R., and Hirakawa, K., *J. Catal.* **63**, 152 (1980).
28. Cotton, F. A., and Wing, R. M., *Inorg. Chem.* **4**, 867 (1965).
29. Hardcastle, F. D., and Wachs, I. E., *J. Raman. Spectrosc.* **21**, 683 (1990); Hardcastle, F. D., and Wachs, I. E., *J. Phys. Chem.* **95**, 10763 (1991).
30. Ueda, W., Morooka, Y., and Ikawa, T., *J. Catal.* **70**, 409 (1981). [Keulks, G. W., and Krenzke, L. D., *in* "Proc. 6th Intern. Congr. Catal., London" (G. C. Bond *et al.*, Eds.), p. 806. Chem. Soc., London, (1976)]
31. Adams, C. R., and Jennings, T. J., *J. Catal.* **3**, 549 (1964).
32. Keulks, G. W., Yu, Z., and Krenzke, L. D., *J. Catal.* **84**, 38 (1983).
33. Cant, N. W., and Hall, W. K., *J. Phys. Chem.* **75**, 2914 (1971).
34. Cant, N. W., and Hall, W. K., *J. Catal.* **22**, 310 (1971).
35. Krenzke, L. D., and Keulks, G. W., *J. Catal.* **61**, 316 (1980).
36. Burrington, J. D., Kartisek, C., and Grasselli, R. K., *J. Catal.* **63**, 235 (1980).
37. Kondo, T., Saito, S., and Tamaru, K., *J. Am. Chem. Soc.* **96**, 6857 (1974).
38. Portefaix, J. L., Figueras, F., and Forssier, M., *J. Catal.* **63**, 307 (1980).
39. Anderson, A. B., Ewing, D. W., Kim, Y., Grasselli, Burrington, J. D., and Brazil, J. F., *J. Catal.* **96**, 222 (1985).
40. Brazdil, J. F., Suresh, D. D., and Grasselli, R. K., *J. Catal.* **66**, 347 (1980).